

Time–quefreny analysis of overlapping similar microseismic events

Koji Nagano

Muroran Institute of Technology, Mizumoto 27-1, Muroran, Hokkaido 050-8585, Japan.

Email: nagano@mmm.muroran-it.ac.jp

Abstract. In this paper, I describe a new technique to determine the interval between P-waves in similar, overlapping microseismic events. The similar microseismic events that occur with overlapping waveforms are called ‘proximate microseismic doublets’ herein. Proximate microseismic doublets had been discarded in previous studies because we had not noticed their usefulness. Analysis of similar events can show relative locations of sources between them. Analysis of proximate microseismic doublets can provide more precise relative source locations because variation in the velocity structure has little influence on their relative travel times. It is necessary to measure the interval between the P-waves in the proximate microseismic doublets to determine their relative source locations.

A ‘proximate microseismic doublet’ is a pair of microseismic events in which the second event arrives before the attenuation of the first event. Cepstrum analysis can provide the interval even though the second event overlaps the first event. However, a cepstrum of a proximate microseismic doublet generally has two peaks, one representing the interval between the arrivals of the two P-waves, and the other representing the interval between the arrivals of the two S-waves. It is therefore difficult to determine the peak that represents the P-wave interval from the cepstrum alone. I used window functions in cepstrum analysis to isolate the first and second P-waves and to suppress the second S-wave. I change the length of the window function and calculate the cepstrum for each window length. The result is represented in a three-dimensional contour plot of length–quefreny–cepstrum data. The contour plot allows me to identify the cepstrum peak that represents the P-wave interval. The precise quefreny can be determined from a two-dimensional quefreny–cepstrum graph, provided that the length of the window is appropriately chosen. I have used both synthetic and field data to demonstrate that this method can be used to identify the cepstrum peak that represents the interval between the arrivals of successive P-waves.

Key words: cepstrum, microseismic events, quefreny, similar events.

Received 15 April 2015, accepted 18 April 2015, published online 15 May 2015

Originally submitted to SEGJ 29 December 2013, accepted 7 January 2015

Introduction

Analysis of similar earthquake events is a seismological tool that has been used to investigate the subsurface structure of the Earth (Poupinet et al., 1984). Events with similar waveforms occur at the same (or proximal) fractures and share a similar source mechanism. The similarity of their sources provides data that can be used to construct precise images of the subsurface fractures.

Analyses of similar seismic events have been used in many geophysical research fields. Cao and Romanowicz (2007) discussed scatterers in the mantle by analysing similar earthquakes. Danesi et al. (2007) reported using similar earthquakes beneath an Antarctic outlet glacier to show the structure of the glacier.

Similar microseismic events also occur during hydraulic injection in fractured reservoir systems, e.g. natural gas reservoirs (Rutledge and Phillips, 2003; Rutledge et al., 2004) and geothermal reservoirs (Moriya et al., 2002; Phillips, 2000). Eisner et al. (2006) reported similar microseismic events that were monitored during hydraulic fracturing in oil and gas fields. Analysis of similar microseismic events has revealed the detailed structure of fractured reservoirs, especially in geothermal fields.

Phillips (2000) analysed similar microseismic events that were induced by hydraulic stimulation of a hot-dry-rock (HDR) geothermal reservoir in the Rhine Graben near Soultz, France. The absolute location of a master event, which was one of

the similar events, was calculated by the conventional arrival-time difference method in advance of the similar event analysis. Relative locations of the sources of events similar to the master event were then calculated by analysing the delay of the coherent frequency components of the similar events. The relative source locations provided a fine image of the fracture reservoir. Subsequently the relative source locations helped to define a fracture network and stress fields that governed fluid flow in the reservoir.

Moriya et al. (2002) used microseismic multiplet analysis in the Soultz HDR field and showed the spatial relationship between hypocenters for similar microseismic events. Combinations of the relative hypocenters of three or more similar events revealed fracture orientations. Moriya et al. (2002) reported that the estimated orientations of the fractures were consistent with the orientation of the tectonic stress field.

Time-dependent change of subsurface structures can also be examined by analyses using similar microseismic events (Poupinet et al., 1996; Yamawaki et al., 2004). Yamawaki et al. (2004) analysed cross-correlation coefficients of pairs of similar earthquakes. They showed that time-dependent cross-correlation patterns of S-waves differed among recording stations. The coefficients determined from two seismograph stations on the slope of Mt. Iwate in Japan decreased with elapsed time and their values became scattered. The

coefficients for stations that were distant from Mt. Iwate were close to 1.0 and were less scattered. This analysis by Yamawaki et al. (2004) showed that the time-dependent cross-correlation patterns of S-waves in the similar earthquakes were indicative of subsurface structural changes caused by volcanic activity at Mt. Iwate.

Similar microseismic events

The analysis of similar microseismic events involves two factors, the difference of the source location and the change of the velocity structure. These two factors are connected to each other. A change of the velocity structure may introduce an error into the source location.

Some mechanisms, e.g. fracture growth, faulting, and metamorphism, will cause a change in the subsurface structure. The intervals between similar events for which analyses have been published in the seismological and geophysical literature range from several seconds to several days (Moriya et al., 2002; Poupinet et al., 1996; Yamawaki et al., 2004; Eisner et al., 2006).

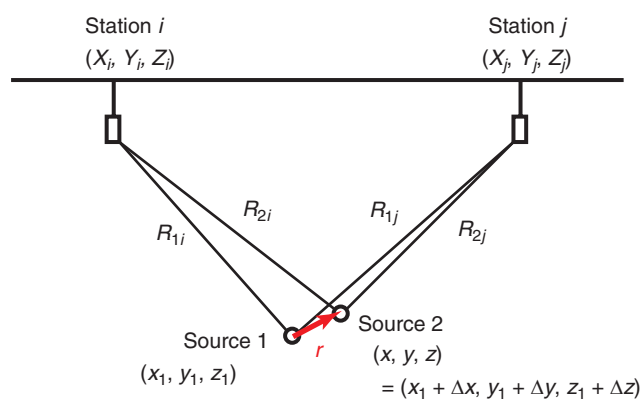


Fig. 1. Schematic representation of estimation of the relative source location r for similar microseismic events. Raypaths are labelled to show sources and recording stations. For example, R_{1i} indicates the raypath from Source 1 recorded at Station i .

If the interval between arrivals is long, the velocity structure may have changed during the interval. For example, when hydraulic fracturing is carried out, fracture growth during the interval between similar events may change the subsurface structure. Block et al. (1994) applied a joint inversion method to monitor hydraulic fracturing. They estimated the velocity structure in combination with source locations by using a joint inversion method. Spreading sources of the microseismic events indicated an active fracture zone. They indicated in their paper that the microseismic events were induced by hydraulic fracturing, and that the velocity structure was changing while the data were collected. Therefore, the source locations should be computed using a time-variant velocity model that includes fracture growth when we analyse microseismic events due to hydraulic fracturing.

We need either P-wave propagation velocity or S-wave propagation velocity, or both, to estimate the relative location of similar sources. The propagation velocities in the field are estimated in advance of the analysis of the arrival-time differences for the source location. The estimation of the P-wave propagation velocity is more reliable than that of the S-wave propagation velocity. Therefore, in this paper, I used only P-wave information to estimate the relative source locations of between the similar microseismic events.

Proximate microseismic doublets

If a second event, with a similar waveform to an earlier event, arrives before complete attenuation of that earlier event, the two events overlap each other. I call such similar events within a short interval 'proximate microseismic doublets'. The interval between proximate microseismic doublets ranges from several hundred milliseconds to several seconds. The interval can depend on the magnitude of an event. Big proximate doublets can have a long interval because of their long duration. The similarity between the two events of the doublet can be estimated from the cepstrum of the overlapping events. The cepstrum of the proximate doublets shows a high, sharp peak at frequency of the interval, which is also estimated by rough observation of the waveform.

We had not previously used proximate microseismic doublets to derive relative source locations. I can offer some reasons why

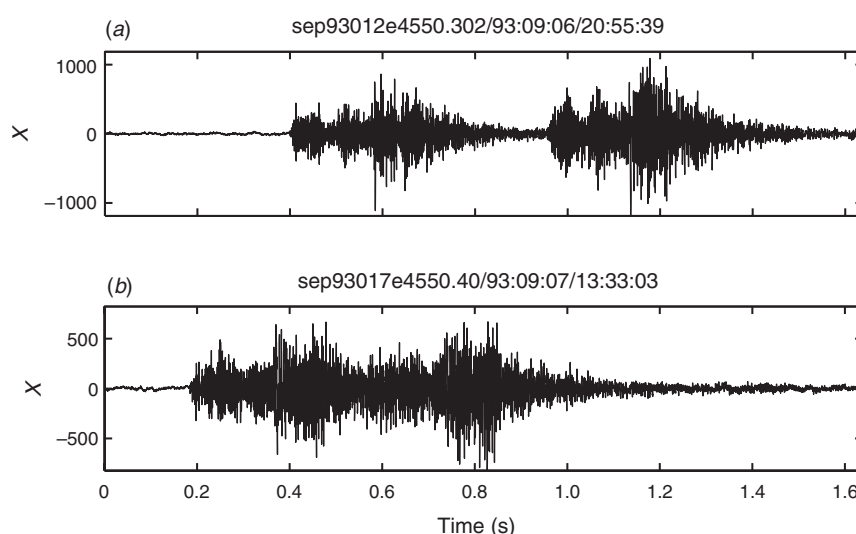


Fig. 2. Waveforms of two proximate microseismic doublets recorded during hydraulic injection at the Soutz HDR field. Two microseismic events of similar waveform were recorded. (a) There is little overlap of the two events. (b) The second event arrives before complete attenuation of the first event. It is therefore difficult to estimate the similarity of the waveforms and to detect the arrival time of the second event.

we had not analysed the proximate microseismic doublets. The first reason is that we had not read of the cepstrum method for estimating the interval. The second reason is the small number of proximate microseismic doublets. However, we can increase the number of estimated source locations by analysing such unused events. Moreover, the location of proximate microseismic doublet sources generally is more precise than that of similar events with a long interval between their origin times. Because the events in a proximate microseismic doublet have a short interval between them, time-dependent changes in the velocity structure should have little effect on the source locations. This possibility of errors for events separated by a long interval was indicated in the combined analysis of source locations and a velocity model by Block et al. (1994). Though proximate microseismic doublets are a small fraction of the events observed, their relative source locations are valuable.

It is difficult to estimate directly the interval between events in proximate microseismic doublets by using time-domain analysis. Bogert et al. (1963) introduced the cepstrum analysis to estimate interval between overlapping events with a similar waveform. The cepstrum shows a clear peak at the interval between similar events. Childers et al. (1977) summarised cepstrum analysis. When we apply cepstrum analysis to a proximate microseismic doublet, two peaks are apparent in their cepstrum. The two peaks are interpreted as the intervals between the P-wave arrivals and the S-wave arrivals. However, the cepstrum does not indicate which peak represents the interval between P-wave arrivals. The two peaks must be identified in order to locate the relative hypocenter. In this paper I present a new analytical method that combines variable length windows with cepstrum analysis to determine the interval between P-wave arrivals in proximate microseismic doublets.

In this paper, I have used microseismic data recorded at the Soutz HDR field during hydraulic fracturing in 1993. A total of 15089 events were located during this fracturing project, of which 6039 were identified as similar microseismic events (Moriya et al., 2002). The recording time for all data files was 1.638 s and the sampling frequency was 5000 Hz.

The cepstrum of a proximate microseismic doublet

In the analysis of the locations of the sources of similar microseismic events, the accuracy of the location of the source of the second event relative to the location of the first is more precise than that estimated by calculating independent source locations for each event (Moriya et al., 2002). The source locations of the first and second events are defined by (x_1, y_1, z_1) and (x, y, z) , respectively. The source location of the second event is also represented by the relative source location $\mathbf{r} = (\Delta x, \Delta y, \Delta z)$,

$$(x, y, z) = (x_1 + \Delta x, y_1 + \Delta y, z_1 + \Delta z). \quad (1)$$

Figure 1 provides a schematic representation of the process described here for estimation of relative source location for similar microseismic events. The absolute source location of the first event, (x_1, y_1, z_1) , is calculated in advance by analysing arrival-time observations among recording stations. The source location, \mathbf{r} , of the source of the second event relative to that of the first event is then calculated from station-to-station observations of arrival-time intervals for the second of the similar events (Ito, 1985).

Examples of proximate microseismic doublets examined in this study are shown in Figure 2. Importantly, the interval between the similar events in Figure 2 is shorter than the duration of a single event.

I found 230 pairs of proximate microseismic doublets in the 15089 events that were observed in the Soutz HDR field (Moriya et al., 2002). I selected waveforms in which two events overlapped by inspection, and made a rough estimate of the interval. We may observe overlapping events with a short interval but which occurred independently. Such overlapping events would not have similar waveforms. When the rough estimate of the interval was close to the queffrequency of the peak in the cepstrum, I concluded that the waveform was likely to be a proximate microseismic doublet (Nagano and Ehara, 2008).

Cepstrum analysis is a method to estimate an interval between two similar event signals, such as in the proximate microseismic doublets. A composite signal consisting of a master wavelet $h(t)$ and its slave signal is represented by

$$g(t) = h(t) + \alpha h(t - \Delta T), \quad (2)$$

where ΔT is the delay between arrivals of the two signals and α is the magnitude ratio between the master and its slave. The power spectrum is

$$|G(f)|^2 = |H(f)|^2 \{1 + \alpha^2 + 2\alpha \cos(2\pi f \Delta T)\}, \quad (3)$$

where $H(f)$ and $G(f)$ are Fourier transforms of $h(t)$ and $g(t)$, respectively. The logarithm of the power spectrum is

$$\log|G(f)|^2 = \log|H(f)|^2 + \log\{1 + \alpha^2 + 2\alpha \cos(2\pi f \Delta T)\}. \quad (4)$$

The inverse Fourier transform of the logarithm of the power spectrum is the cepstrum, which is a function of queffrequency (Bogert et al., 1963; Childers et al., 1977; Brockwell and Davis, 2002). The dimension of queffrequency is time. The

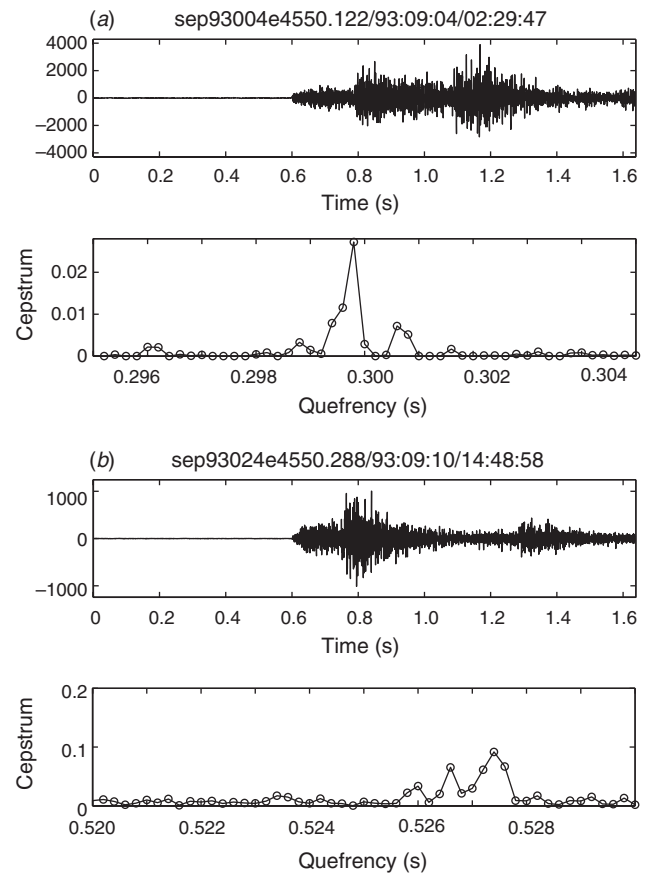


Fig. 3. Waveforms and cepstra for two proximate microseismic doublets, shown with an expanded time scale. The two peaks representing the intervals between successive P- and S-wave arrivals are clearly evident in the cepstra.

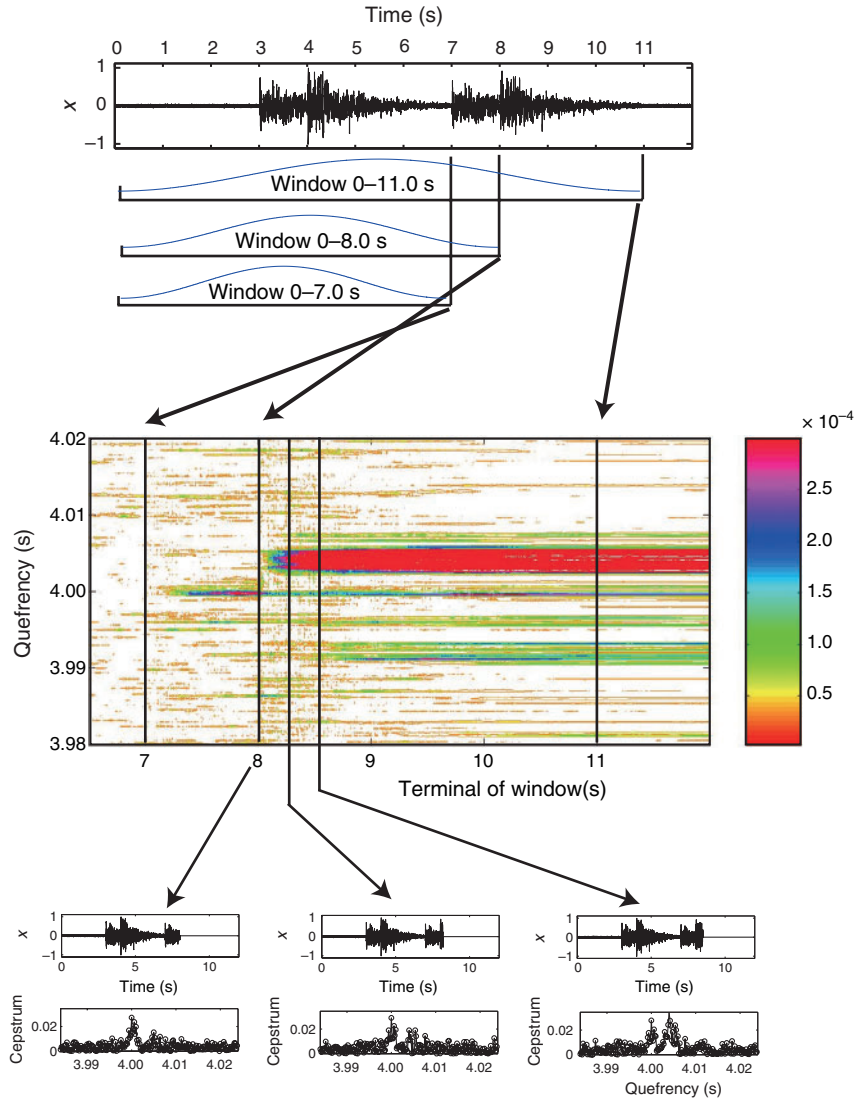


Fig. 4. Conceptual methodology of time–quefreny analysis for detection of the interval between successive P-wave arrivals of proximate microseismic doublets.

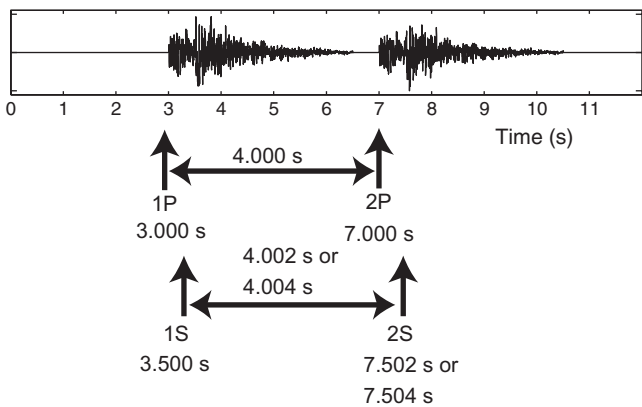


Fig. 5. Parameters defining the synthesised signals used to simulate proximate microseismic doublets in this study.

cepstrum of Equation 2 shows a distinct peak at a quefreny of ΔT because there is an additive periodic component, $\log\{1 + \alpha^2 + 2\alpha \cos(2\pi f \Delta T)\}$, in Equation 4.

Cepstrum analysis of proximate microseismic doublets is more complex than that represented by the pair of wavelets of

Equation 2. Each seismic event has both a P-wave component and an S-wave component. Therefore, there are two pairs of overlapping seismic waves in proximate microseismic doublets. A composite signal $y(t)$, which represents proximate microseismic doublets, is

$$y(t) = x_P(t) + x_S(t) + \alpha x_P(t - \Delta T_P) + \alpha x_S(t - \Delta T_S), \quad (5)$$

where $x_P(t)$ and $x_S(t)$ are the P- and S-waves, respectively, of the first event, and ΔT_P and ΔT_S are intervals between P- and S-wave arrivals, respectively, for the two similar events. Fourier transforms of $x_P(t)$ and $x_S(t)$ are defined as $X_P(f)$ and $X_S(f)$, respectively. The logarithm of the power spectrum of $y(t)$ in Equation 5 is

$$\begin{aligned} \log |Y(f)|^2 = & \log [|X_P(f)|^2 \{1 + \alpha^2 + 2\alpha \cos(2\pi f \Delta T_P)\} \\ & + |X_S(f)|^2 \{1 + \alpha^2 + 2\alpha \cos(2\pi f \Delta T_S)\} \\ & + 2|X_P(f)||X_S(f)|\alpha \times \cos\{\theta_P(f) - \theta_S(f) - 2\pi f \Delta T_P\} \\ & + 2|X_P(f)||X_S(f)|\alpha \times \cos\{\theta_P(f) - \theta_S(f) - 2\pi f \Delta T_S\} \\ & + 2|X_P(f)||X_S(f)|\alpha^2 \times \cos\{\theta_P(f) - \theta_S(f) \\ & - 2\pi f(\Delta T_P - \Delta T_S)\} \\ & + 2|X_P(f)||X_S(f)| \cos\{\theta_P(f) - \theta_S(f)\}]. \end{aligned} \quad (6)$$

Therein, $X_P(f) = |X_P(f)| \exp\{j\theta_P(f)\}$, $X_S(f) = |X_S(f)| \exp\{j\theta_S(f)\}$, and $\theta_P(f)$ and $\theta_S(f)$ are the phase spectra of the P- and S-waves, respectively. Equation 6 contains periodic components. Consequently, the cepstrum of Equation 5 will exhibit two peaks at intervals of ΔT_P and ΔT_S .

Figure 3 shows portions of the cepstra of two examples of proximate microseismic doublets. The sampling frequency constrains the quefrequency resolution in the cepstrum. Because the sampling frequency is 5000 Hz in Figure 3, the quefrequency resolution is 0.2 ms. Two peaks are clearly visible in the cepstra shown in Figure 3. For example, we can see the two peaks at 0.2998 s and 0.3006 s in Figure 3a. However, which peak represents the P-wave delay cannot be determined by using only the information shown in Figure 3.

Time-quefrequency analysis

I have devised a further analysis of the cepstrum for proximate microseismic doublets. During the cepstrum analysis, it would be desirable to attenuate the peak that represents the S-wave interval to enhance the cepstrum peak of the P-wave interval. If the data after the arrival of the second S-wave were replaced with zeros, the S-wave signals would lose similarity. Consequently the cepstra of the modified data should show a decrease in the magnitude of the peak representing the interval between the S-waves.

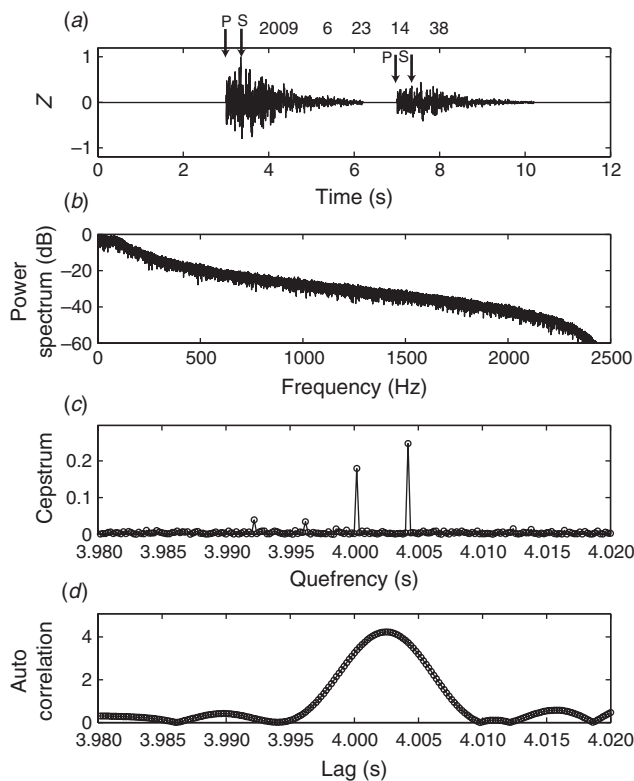


Fig. 6. Analysis of a noise-free, synthesised signal simulating proximate microseismic doublets. (a) Time-domain display of the synthetic waveform showing arrival times of P- and S-waves. The intervals between P- and S-waves were 4.000 s and 4.004 s, respectively. (b) Power spectrum of the synthesised signal. Note that it is not white. (c) Cepstrum of the synthesised signal showing two well defined peaks corresponding to the intervals between successive P- and S-wave arrivals. (d) Autocorrelation of the synthesised signal. The broad peak spanning the intervals between P- and S-wave arrivals by autocorrelation.

I use a window function in the cepstrum analysis. The window function is intended to exclude the second S-wave and to suppress the similarity between the S-waves. The length of the window function is varied so that we can see the effect of the window length on the cepstra. Because the cepstrum is a non-linear transformation and there are two waves in the data, the effect on the cepstrum of the multiplied window function is not simple. We can discriminate the peak representing the S-wave interval from that representing the P-wave interval in the cepstra by repetitive application of this window function with varying window length. I call this method 'time-quefrequency analysis'. I use the Hamming window in my analysis to reduce bias due to spectral leakage in the estimation of the power spectrum (Percival and Walden, 1998).

Time-quefrequency analysis performed as follows. Figure 4 illustrates time-quefrequency analysis and ways of representing its results. The window begins at the start of the doublet record, but the end or terminal time (T_w) of the window is systematically shifted from before the second P-wave arrival to the end of the second S-wave. The contour plot in Figure 4 shows the cepstrum for each window terminal time and quefrequency. Two notable cepstrum peaks are observed, one commencing at a terminal time of just over 7 s, and the second at a terminal time of just over 8 s. The cepstrum peak at a quefrequency of ~ 4.004 s corresponds to the S-wave interval and the peak at ~ 4.000 s corresponds to the P-wave interval. The peak corresponding to the P-wave interval starts at ~ 7.2 s and continues to 12 s. On the other hand, the peak corresponding

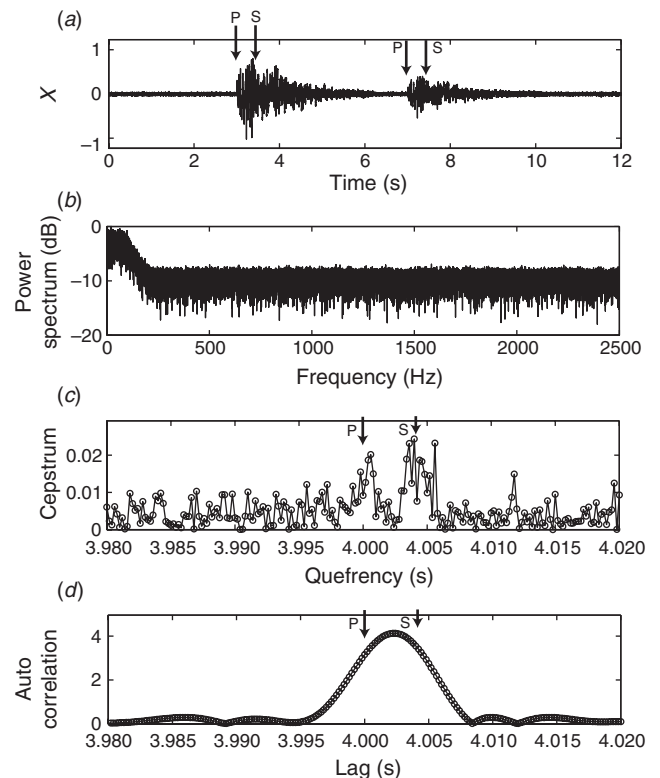


Fig. 7. Analysis of a synthesised signal with noise added. (a) Time-domain display of the synthetic waveform showing arrival times of P- and S-waves. (b) Power spectrum of the synthesised signal. The flat power spectrum in the high-frequency range is caused by the added noise. Low-frequency components are dominant. (c) Cepstrum of the synthesised signal showing two peaks corresponding to the intervals between successive P- and S-wave arrivals. The peaks are broader and less well defined than those of the noise-free data of Figure 6c. (d) Autocorrelation of the synthesised signal showing a broad peak similar to that of Figure 6d.

to the S-wave interval starts after ~ 8 s. It is because, for window lengths less than 8 s, the energy of the second S-wave is excluded by the multiplied window function and so does not contribute to the cepstrum.

It is difficult to determine the precise quefrequency of the P-wave interval from only the contour plot because a sharp top of the peak is not clearly visible in the contour plot. I therefore produced two-dimensional cepstrum–quefrequency graphs from

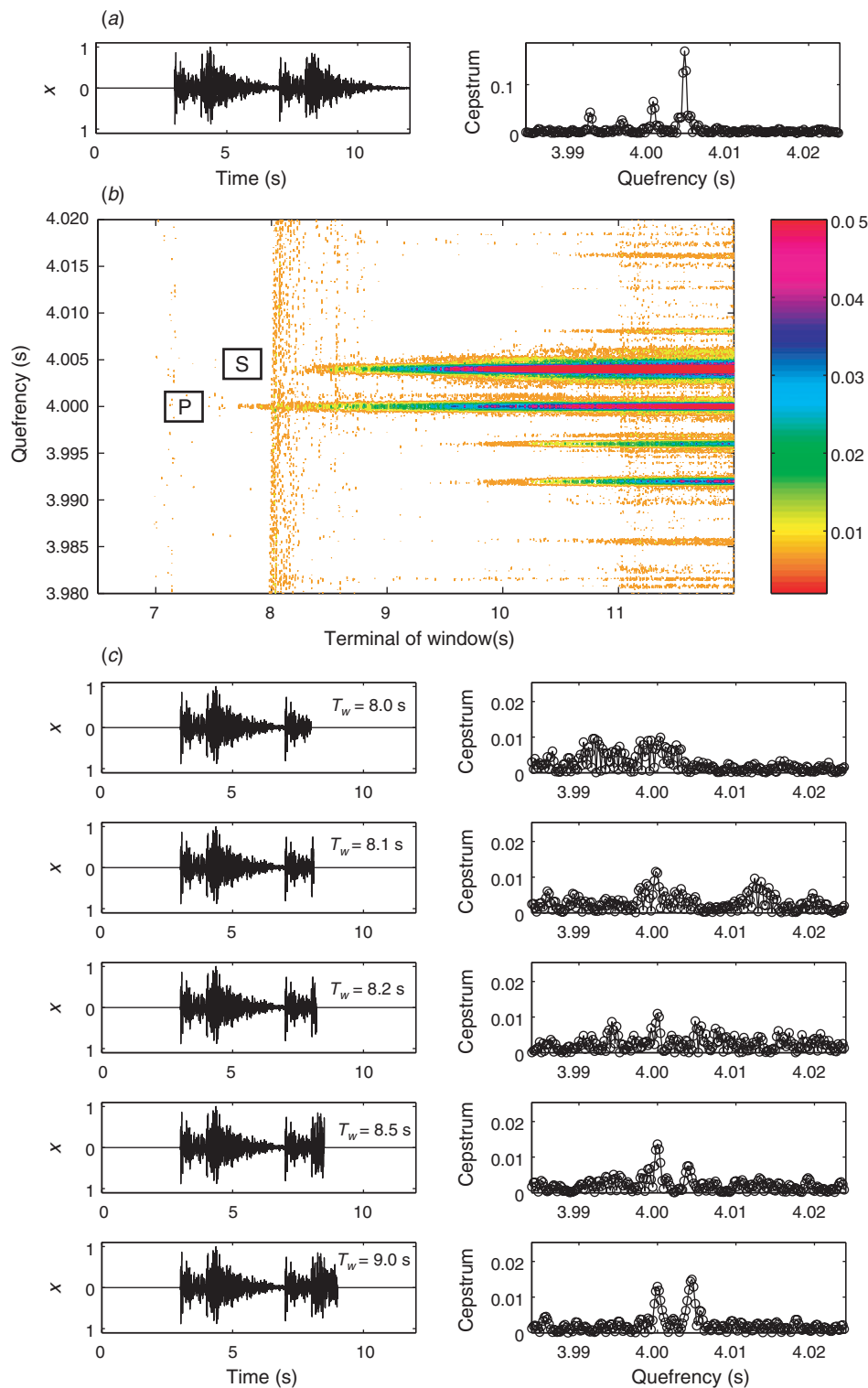


Fig. 8. Time–quefrequency analysis for a noise-free synthesised signal. (a) Full waveform and its cepstrum. (b) Contour plot of cepstrum as a function of quefrequency and time window. Two peaks are evident at quefrequencies representing the intervals between successive P- and S-wave arrivals. (c) Cepstra for selected time windows from the contour plot of (b). T_w is the window length ('terminal') of the window. Data after the arrival of the second S-wave include part of the coda of the second P-wave. Therefore, the similarity of the P-wave also decreases as well as that of the S-wave when the data after the second S-wave is deleted. The peak of the P-wave interval also varies in the cepstrum when data after the arrival of the second S-wave are excluded.

the three-dimensional time–quefrequency–cepstrum data. The quefrequency of the P-wave interval is conclusively determined in the cepstra as shown in the bottom panel of Figure 4.

The window length variation also affects the peak of the P-wave interval in the cepstra of a proximate microseismic doublet. The second S-wave arrives during the coda part of the second P-wave, so we observe both contributions simultaneously. When data after the arrival of the second S-wave are excluded, the contribution from the coda part of the second P-wave is also

excluded. Therefore, the cepstrum peak due to the P-wave interval will be affected. Because the energy in the coda of the second P-wave is smaller than the energy in the initial part of the second S-wave, the S-wave interval peak is not greatly affected.

Computer simulation

I conducted time–quefrequency analyses using synthesised signals that simulated proximate microseismic doublets. Figure 5 shows

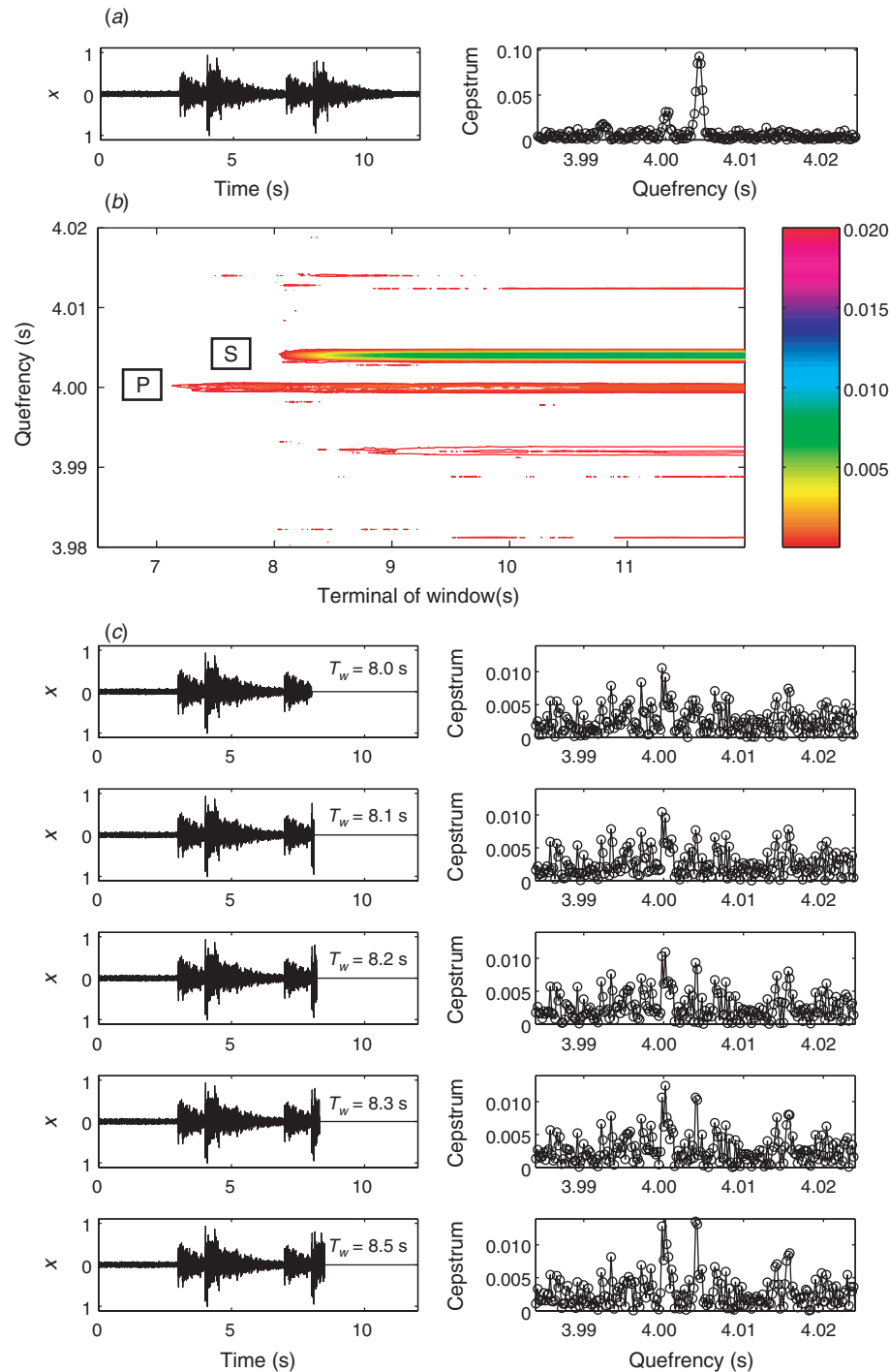


Fig. 9. Time–quefrequency analysis for the synthesised signal of Figure 8 with noise added so that the signal-to-noise ratio is lower than that of Figure 8. (a) Full waveform and its cepstrum. (b) Contour plot of cepstrum as a function of quefrequency and time window. The two peaks are less well defined than those of Figure 8. Artefacts appear around the true peaks. Because the artefacts are smaller than the true peaks, they can be isolated from the true ones. (c) Cepstra for selected time windows from the contour plot of (b). T_w is the terminal of the window.

the waveform used for the numerical simulation together with the parameters that define the waveform. A signal simulating a microseismic event consists of two series of Gaussian random numbers that decreased exponentially. The two series simulate P- and S-waves, respectively. The Gaussian series are filtered to

suppress high-frequency components because low-frequency components are dominant in a real seismic event. The cut-off frequency of the low-pass filter is 100 Hz. I then add a second signal, which is similar to the first signal, with a time lag to simulate a proximate microseismic doublet. I add another series

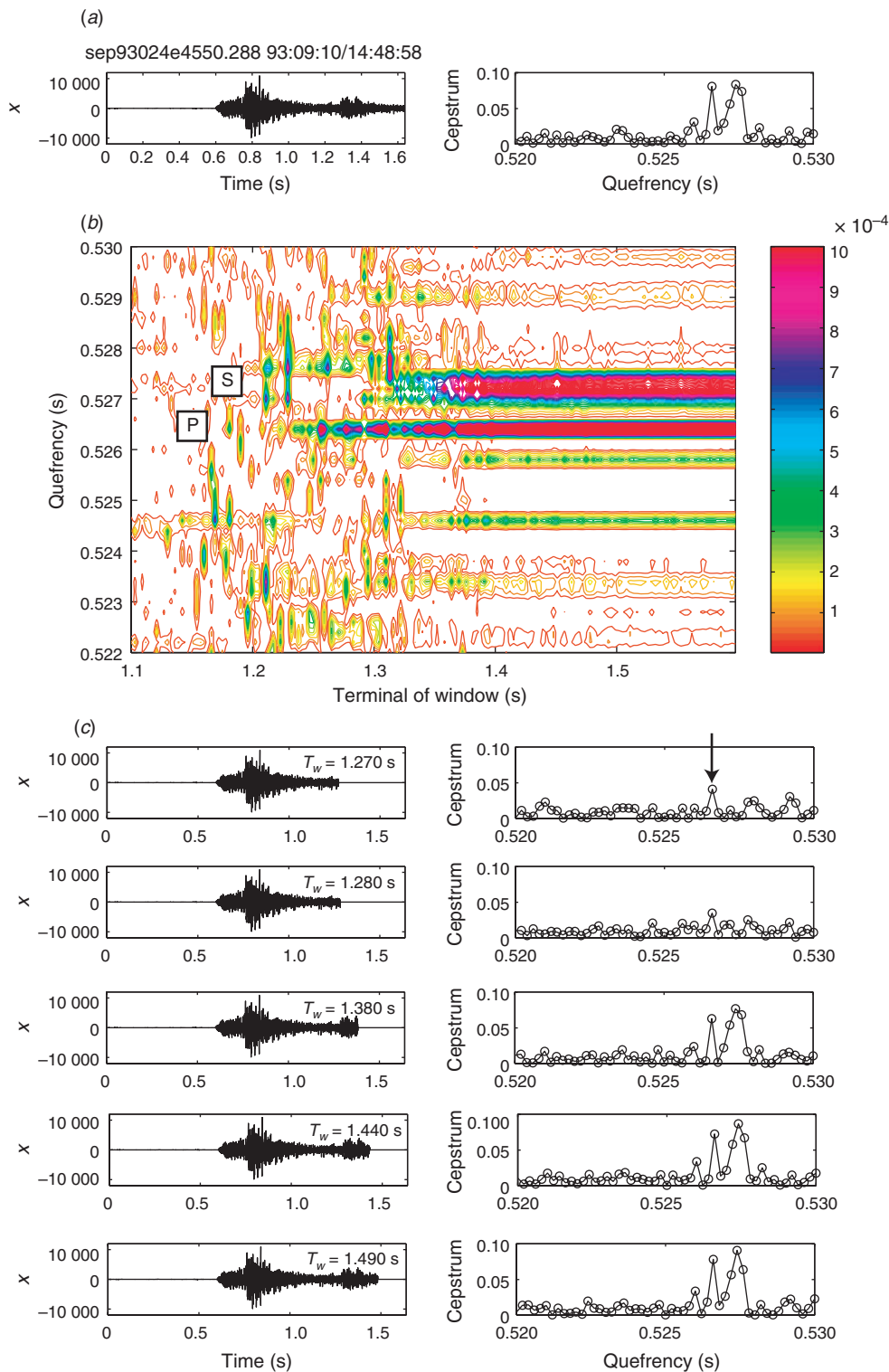


Fig. 10. First example of a time–quefrequency analysis for a proximate microseismic doublet recorded at the Soultz HDR field. (a) Full waveform and its cepstrum. Two peaks are observed in the cepstrum. (b) Contour plot of cepstrum as a function of quefrequency and time window. The peak that starts earlier represents the interval between successive P-wave arrivals. (c) Cepstra for selected time windows from the contour plot of (b). The arrow indicates the cepstral peak that represents the interval between arrivals of successive P-waves. T_w is the terminal of the window.

of Gaussian random numbers to the simulated event to model background noise. Sampling frequency was set to 5000 Hz. The interval between P-waves was 4.000 s and that between S-waves was 4.004 s. The difference between these intervals is 20 sample points for a sampling frequency of 5000 Hz.

Figures 6 and 7 show spectra, cepstra and autocorrelations of the synthesised signals. The synthesised signal of Figure 6 has no noise, and its cepstrum shows distinct peaks at the

queffrequency corresponding to the interval between successive P-waves and that between successive S-waves (Figure 6c). Figure 7 shows the cepstrum of the synthesised signal with noise added. The cepstrum again has peaks at the queffrequencies corresponding to the P-wave and S-wave intervals (Figure 7c); however, the peaks are wider and their forms less clear than those of the noise-free signals. Autocorrelation analysis also provides an interval between arrival-times for the synthesised

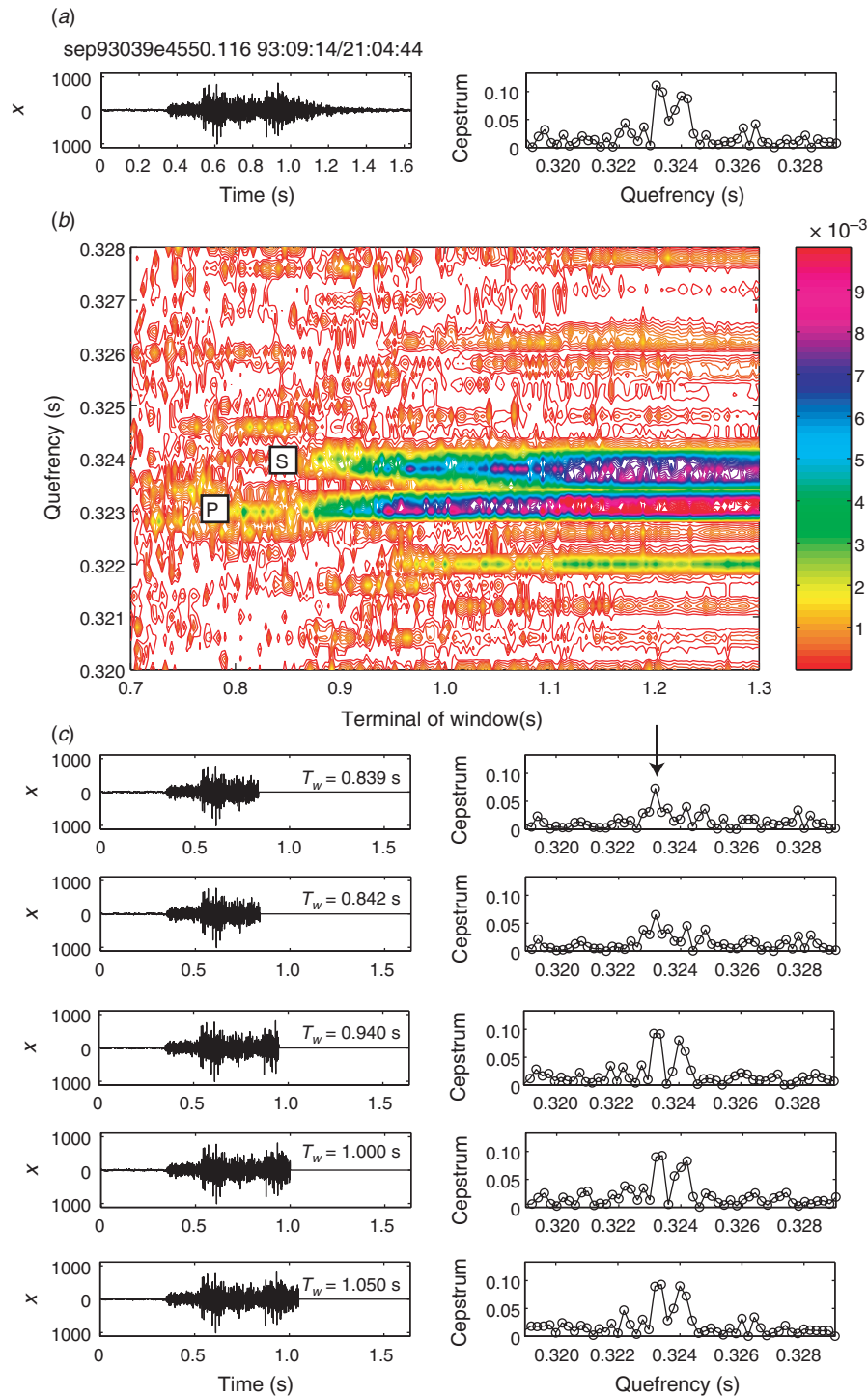


Fig. 11. Second example of a time-queffrequency analysis for a proximate microseismic doublet recorded at the Soultz HDR field. (a) Full waveform and its cepstrum. Two peaks are observed in the cepstrum. (b) Contour plot of cepstrum as a function of queffrequency and time window. The peak at the queffrequency of 0.323 s is longer than that of 0.324 s. Therefore, the peak at the queffrequency of 0.323 s represents P-wave. (c) Cepstra for selected time windows from the contour plot of (b). T_w is the terminal of the window.

signal; however, the resolution of this method is lower than that of cepstrum analysis because the spectra of the synthesised signals are not white (Brockwell and Davis, 2002).

Figure 8 shows the result of time–quefrequency analysis for a synthesised signal with no noise. The contour plot of Figure 8*b* shows two main peaks at the quefrequencies of 4.000 s and 4.004 s.

The cepstrum peak at the earlier start time represents the interval between P-wave arrivals. The cepstra profiles of Figure 8*c* show the interval between the P-waves more precisely than in the contour plot (Figure 8*b*).

Some further peaks are visible in the contour plot, e.g. at the quefrequencies of ~3.996 s, 3.992 s, and 3.985 s, when the window

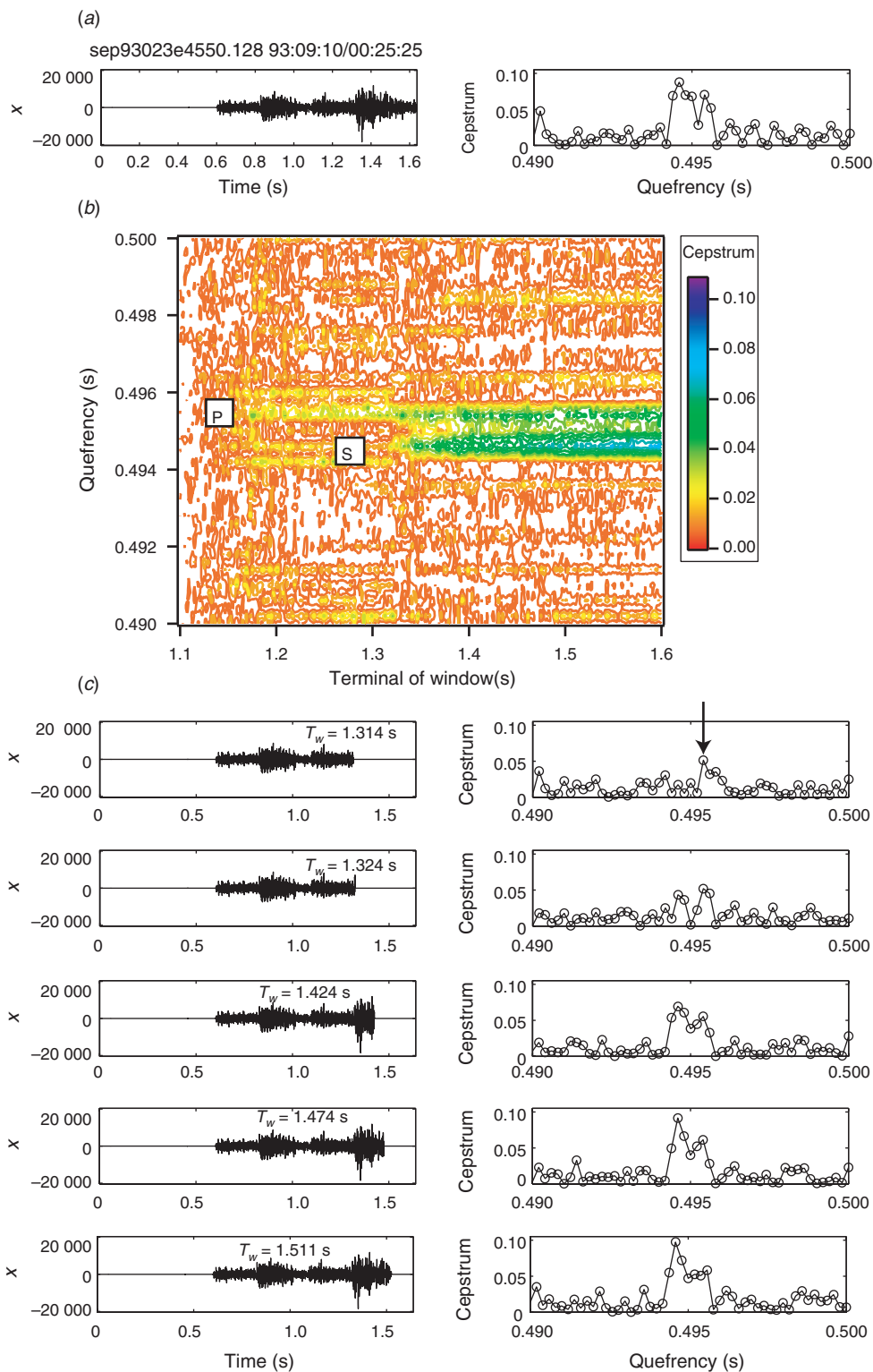


Fig. 12. Third example of a time–quefrequency analysis for a proximate microseismic doublet recorded at the Soultz HDR field. (a) Full waveform and its cepstrum. Two peaks are observed in the cepstrum. (b) Contour plot of cepstrum as a function of quefrequency and time window. Two peaks conserve on a single peak after 1.5 s. (c) Cepstra for selected time windows from the contour plot of (b). The arrow indicates the cepstral peak that represents the interval between arrivals of successive P-waves. T_w is the terminal of the window.

length is greater than 10 s. I can conclude the above mentioned peaks are artefacts because we cannot find any onsets of the events in Figure 8a at the starting time of the peaks in the contour plot of Figure 8b.

Figure 9 shows the time–quefreny analysis result for synthetic data with Gaussian noise. In the contour plot of Figure 9b, the relationship of the start times of the peaks is again confirmed. However, by when comparing Figure 9c with Figure 8c, we find that the true peaks corresponding to the intervals of P- and S-waves are contaminated by many noisy peaks. Therefore, it is difficult to recognise the true peaks from Figure 9c only. However, we can recognise them by comparing the contour plot of Figure 9b with Figure 9c. Using the cepstrum–quefreny graphs alone sometimes does not provide good results because of the noise contamination. Therefore, comparison the cepstrum–quefreny graphs with the contour plot is important for accurate recognition of the true peaks.

As shown in Figures 8 and 9, the cepstrum often has artefacts near true peaks. The cepstrum has higher-order components (Childers et al., 1977), which are artefacts of the true cepstrum peaks. However, the artefacts caused by the higher-order components are smaller than the true cepstrum peaks (Childers et al., 1977). For example, peaks shown at the quefreny of 3.996 and 3.992 s in Figure 8b and at the quefreny of 3.99 s in Figure 9b are the artefacts. The magnitudes of these peaks are smaller than the true peaks, however. We can get a rough estimate of the interval based on the observation of the waveform. We can isolate the artefacts in the contour plot by using both this rough estimate of the interval and the smaller amplitude property of the higher-order cepstrum components.

Field data analysis

I used the time–quefreny technique described above to analyse proximate microseismic doublets that were recorded at the Soutz HDR field. My aim was to detect the interval between P-waves within the recorded data. Figures 10–12 illustrate the results representing a contour plot and five cepstra for selected time window functions in each figure.

Application of the time–quefreny technique successfully determined the intervals between P-wave arrivals for the proximate microseismic doublets shown here, which were recorded at the Soutz HDR field. Two peaks and the difference of their start times were recognisable in the contour plots for the real data. The contour plot of Figure 10 shows peaks at quefrenies of 0.5264 s and 0.5275 s. The earlier peak represents the interval between P-wave arrivals in the contour plot of Figure 10. We can also recognise two peaks at quefrenies of 0.323 s and 0.324 s in the contour plot of Figure 11. The peak at the quefreny of 0.323 s starts earlier than another peak.

The shape of the peaks in the contour plot of Figure 12 differs from that of the peaks shown in Figures 10 and 11. Two peaks are again evident, at quefrenies of 0.4945 s and 0.4955 s before the window terminal time of ~1.37 s. It is difficult to recognise the two peaks after the window terminal time of 1.5 s in the contour plot of Figure 12b. However, we can see two peaks in the cepstrum of the Figure 12c. The peak at the quefreny of 0.4955 s starts at a smaller window terminal time than other peaks. Therefore, the peak at the quefreny of 0.4955 s represents the interval between successive P-waves.

As was the case for the synthetic data, the cepstrum–quefreny graphs for the real proximate microseismic doublets (Figures 10c, 11c, and 12c) allow more precise determination of the quefreny representing the interval between P-wave arrivals than the contour plots. The P-wave peaks are indicated by arrows in Figures 10c–12c.

It is important to set an appropriate length of the time window when the cepstrum–quefreny graphs, as shown in Figures 10c and 11c, are produced. For example, in Figure 11c, the cepstra of $T_w = 0.940$ s, 1.000 s, and 1.050 s show two peaks. But it is difficult to identify two peaks in the cepstra of $T_w = 0.839$ s or 0.842 s. If we analyse only the cepstrum of $T_w = 0.839$ s to determine exact quefrenies, we cannot determine them. Also, the peak in the cepstrum–quefreny graph might be poorly resolved if the window length is not appropriate for the data. Therefore, it is important to compare some cepstrum–quefreny graphs so that the appropriate length of the time window can be selected.

Conclusions

The interval between P-waves arrivals in proximate microseismic doublets can be detected by using time–quefreny analysis. In such an analysis, the cepstra show two peaks that represent the intervals between successive P-wave and S-wave arrivals. I examined some features of the time–quefreny analysis by computer simulation using synthesised signals, and then applied the technique to field data recorded at the Soutz HDR field.

My computer simulations showed that cepstra provide higher resolution estimates of arrival-time intervals than autocorrelations, and that noise added to the synthesised signal widens the cepstral peaks. The computer simulations also showed that cepstra derived from time–quefreny analysis, in which a window function is used to exclude the second S-wave, can identify the interval between two P-waves of proximate microseismic doublets. Even though the signal-to-noise ratio was low, and the cepstrum showed a broad peak that covered both the P-wave and S-wave intervals, I was able to identify the peak representing the interval between P-waves in contour plots of time–quefreny–cepstrum data.

I also applied my time–quefreny analysis to proximate microseismic doublets recorded at the Soutz HDR field and demonstrated that the technique can be successfully applied to real data.

We can determine the relative location of the sources of proximate microseismic doublets when the P-wave interval, which is determined by using the time–quefreny analysis, can be compared among four stations. Therefore, this paper has settled the first stage of the problem of relative source location for proximate microseismic doublets.

I have pointed out some practical techniques of time–quefreny analysis as we have applied it to synthesised and real data. The cepstrum of microseismic waveforms is often contaminated by artefacts and noisy peaks that are produced in the calculation of the cepstrum. To overcome the contamination and estimate precise interval with high resolution, it is important to do complementary analyses of the contour plot of the time–quefreny analysis, the cepstrum, and the waveform.

Acknowledgements

I thank staff at Socomine and Dr Hirokazu Moriya (Tohoku University) for their help and for providing access to the microseismic data used in this study. This work was carried out under a Japanese Ministry of Education, Culture, Sports, Science and Technology Grant-in-Aid (No. 20560753) for Scientific Research (C).

References

- Block, L. V., Cheng, C. H., Fehler, M. C., and Phillipe, W. S., 1994, Seismic imaging using microearthquakes induced by hydraulic fracturing: *Geophysics*, **59**, 102–112.

- Bogert, B. P., Healy, M. J., and Tukey, J. W., 1963, The quefrency analysis of time series for echoes: cepstrum, pseudo-autocovariance, cross-cepstrum, and saphe cracking, in M. Rosenblatt, ed., *Time series analysis*: Wiley, 209–243.
- Brockwell, P. J., and Davis, R. A., 2002, *Introduction to time series and forecasting*: Springer-Verlag.
- Cao, A., and Romanowicz, R., 2007, Locating scatterers in the mantle using array analysis of PKP recursors from an earthquake doublet: *Earth and Planetary Science Letters*, **255**, 22–31. doi:10.1016/j.epsl.2006.12.002
- Childers, D. G., Skinner, D. P., and Kemerait, R. C., 1977, The cepstrum: a guide to processing *Proceedings of the IEEE*, **65**, 1428–1443. doi:10.1109/PROC.1977.10747
- Danesi, S., Bannister, S., and Morelli, A., 2007, Repeating earthquakes from rupture of an asperity under an Antarctic outlet glacier: *Earth and Planetary Science Letters*, **253**, 151–158. doi:10.1016/j.epsl.2006.10.023
- Eisner, L., Fischer, T., and Le Calvez, J. H., 2006, Detection of repeated hydraulic fracturing (out-of zone growth) by microseismic monitoring: *The Leading Edge*, **25**, 548–554. doi:10.1190/1.2202655
- Ito, A., 1985, High resolution relative hypocenters of similar earthquakes by cross-spectral analysis method: *Journal of Physics of the Earth*, **33**, 279–294. doi:10.4294/jpe1952.33.279
- Moriya, H., Nakazato, K., Niitsuma, H., and Baria, R., 2002, Detailed fracture system of the Soultz-sous-Forêts HDR field evaluated using microseismic multiplet analysis: *Pure and Applied Geophysics*, **159**, 517–541. doi:10.1007/PL00001263
- Nagano, K., and Ehara, D., 2008, Automatic detection of proximity AE doublets for relative location of subsurface fracture reservoir: *Institute of Electrical Engineers of Japan Transactions on Electronics, Information and Systems*, **128**, 1005–1010. [in Japanese]
- Percival, D. B., and Walden, A. T., 1998, *Spectral analysis for physical applications*: Cambridge University Press.
- Phillips, W. S., 2000, Precise microearthquake locations and fluid flow in the geothermal reservoir at Soultz-sous-Forêts, France: *Bulletin of the Seismological Society of America*, **90**, 212–228. doi:10.1785/0119990047
- Poupinet, G., Ellsworth, W. L., and Frechet, J., 1984, Monitoring velocity variations in the crust using earthquake doublets: an application to the Calaveras fault, California: *Journal of Geophysical Research*, **89**, 5719–5731. doi:10.1029/JB089iB07p05719
- Poupinet, G., Ratdomopurbo, A., and Coutant, O., 1996, On the use of earthquake multiplets to study fractures and the temporal evolution of an active volcano: *Annali di Geofisica*, **39**, 253–264.
- Rutledge, J. T., and Phillips, W. S., 2003, Hydraulic stimulation of natural fractures as revealed by induced microearthquakes, Carthage Cotton Valley gas field, east Texas: *Geophysics*, **68**, 441–452. doi:10.1190/1.1567214
- Rutledge, J. T., Phillips, W. S., and Mayerhofer, M. J., 2004, Faulting induced by forced fluid injection and fluid flow forced by faulting: an interpretation of hydraulic-fracture microseismicity, Carthage Cotton Valley gas field, Texas: *Bulletin of the Seismological Society of America*, **94**, 1817–1830. doi:10.1785/012003257
- Yamawaki, T., Nishimura, T., and Hamaguchi, H., 2004, Temporal change of seismic structure around Iwate volcano inferred from waveform correlation analysis of similar earthquakes: *Geophysical Research Letters*, **31**, L24616. doi:10.1029/2004GL021103